AIAA JOURNAL
Vol. 61, No. 9, September 2023

Quantifying How Turbulence Enhances Boundary Layer Skin Friction and Surface Heat Transfer

Armin Kianfar*
University of California, Irvine, California 92697
Ahmed Elnahhas†
Stanford University, Stanford, California 94305
and
Perry L. Johnson‡
University of California, Irvine, California 92697

https://doi.org/10.2514/1.J063042

Transitional and turbulent boundary layer (BL) flows possess dramatically larger wall-shear stresses and surface heat fluxes than their laminar counterparts. Locally, this can be explained by appealing to the presence of spatiotemporally coherent velocity and temperature regions that enhance the momentum and thermal transport across the BL. However, these coherent structures are seldom present alone, but usually influenced by other physical phenomena, such as the streamwise growth of BLs or freestream pressure gradients. A moment of enthalpy integral equation is introduced to quantify how turbulence and other flow phenomena enhance surface heat flux. Results from a direct numerical simulation of a transitional and turbulent BL are used to demonstrate the proposed analysis method and to form a quantitative assessment of the BL physics. The integral analysis demonstrated in this paper for canonical turbulent flows provides an interpretable analysis tool for unlocking key BL physics, including future extensions to compressible BLs, freestream pressure gradients, and the evaluation of flow control schemes.

Nomenclature

C_f = skin friction coefficient
ℓ = distance from wall about which moments are taken
P_∞ = freestream pressure
p = pressure
q_w = surface heat flux
U_∞ = freestream velocity
u = streamwise velocity
St = Stanton number
T = temperature
T_w = wall temperature
T_∞ = freestream temperature
v = wall-normal velocity
x = streamwise coordinate
y = wall-normal coordinate
α = thermal diffusivity
δ_{99} = 99% boundary-layer thickness
δ^* = displacement thickness
θ = momentum thickness
θ_ℓ = angular momentum thickness
θ_v = wall-normal momentum thickness
δ^h = enthalpy thickness
δ^h_ℓ = moment of enthalpy thickness
δ^h_v = wall-normal enthalpy thickness
ν = kinematic viscosity
ρ = density
τ_w = wall shear stress
$\overline{(\cdot)}$ = Reynolds-averaged quantity

Presented as Paper 2022-0944 at AIAA SciTech 2022 Forum, San Diego, CA, and Virtual, January 3–7, 2022; received 30 March 2023; accepted for publication 26 April 2023; published online 30 May 2023.

*Researcher, Mechanical & Aerospace Engineering, 4200 Engineering Gateway.
†Graduate Researcher, Center for Turbulence Research, 481 Panama Mall. Member AIAA.
‡Assistant Professor, Mechanical & Aerospace Engineering, 4200 Engineering Gateway. Member AIAA.

I. Introduction

TRANSITION to turbulence in boundary layers (BLs) is accompanied by a significant jump in the surface friction and heat transfer [1]. In the late stage of the transition, before turbulence is fully developed, BLs experience a peak surface friction and heat flux [2–4]. Depending on the application, this may be beneficial or deleterious (or both).

The qualitative understanding of the BL transition to turbulence on the skin friction and heat transfer enhancement is very well established for wall-bounded flows. During the transition to turbulence the rate at which momentum and heat is transported across the BL increases substantially compared with the molecular fluxes responsible for such transport in laminar BLs. Because BLs develop with downstream distance, other physical flow phenomena, including fluctuations, may also alter momentum and heat fluxes at the wall. For instance, the mean wall-normal velocity plays a role in transport and the rate at which the BL thickens. Furthermore, externally imposed pressure gradients can dramatically alter the skin friction and surface heat flux, even leading to a BL separation in the case of strong adverse pressure gradients [5]. While such a qualitative understanding of these effects is quite intuitive, a quantitative mathematical mapping between the flow phenomena involved during the transition and to what extent they alter the surface friction and heat transfer is desirable for engineering design analysis such as flow control optimization [6,7] and the interpretation of wall measurements [8].

For fully developed internal flows such as channel or pipe flows, a triple integration (or equivalently, a second moment integral) of the mean momentum equation provides a simple method for quantifying the effect of Reynolds stresses on the friction factor compared to an equivalent laminar flow [9,10]. In a subsequent study, the generalized form of the Fukagata-Iwamoto-Kasagi (FIK) equation for three-dimensional complex wall shapes was introduced [11]. It is also of a significant interest to study the heat transfer in transitional and turbulent BLs. Therefore, the FIK approach has been extended to the case of heat transfer in internal flows [12]. In terms of applications, for instance, the FIK method provided an important guidance on the limitation of flow control schemes in the context of internal flows [13]. For incompressible BLs, several derivations of the FIK equation were developed based on the triple integration [14,15]. Interestingly,

the weighting of the Reynolds shear stress term in the resulting integral equation shows that turbulent fluctuations near the wall are more influential in the friction factor enhancement than those closer to the centerline. Instead of triple integration, a twofold repeated integration was proposed to remove the wall-normal distance weighting for incompressible turbulent BLs [16]. However, in FIK equation for BLs and its variants based on twofold integration, the viscous term does not represent the laminar skin friction, i.e., Blasius solution [17], for incompressible BLs. In other words, when applied to BLs, the FIK relation loses the clean interpretation they enjoyed for internal flows, and existing approaches do not entirely set the matter straight. For instance, they do not yield the friction turbulent enhancement relative to an equivalent laminar BL at a matching Reynolds number.

Another approach to decompose the skin friction of turbulent BLs was introduced by Renard and Deck [18], who proposed an equation established on the budget of the mean flow kinetic energy. This so-called RD equation emphasizes the energetics of the BL, including the prominent role of the logarithmic layer. The interpretation of the RD equation for BLs is quite different from the original FIK relation for internal flows, however, because the influence of turbulence on the mean velocity profile (and its gradient) is included in the viscous term. Thus, the resulting relation does not delineate between laminar and turbulent skin friction, in the sense that the skin friction of an equivalent laminar BL is not represented (as in the original FIK for internal flows). Thus, it does not form a unified conceptual framework with FIK.

Recently, Elnahhas and Johnson [19] developed the angular momentum integral (AMI) equation by integrating the first moment of momentum deficit equation for incompressible BLs. The AMI equation accomplishes for BLs what the FIK equation does for internal flows (pipes, channels). Specifically, it relates the skin-friction coefficient of any (e.g., turbulent) BL to the sum of an equivalent laminar skin-friction coefficient (as a function of a user-defined Reynolds number) plus an (unweighted) integral of the Reynolds shear stress, along with other terms (e.g., freestream pressure gradients). In addition to the clear mathematical interpretation as enhancement or attenuation relative to an equivalent laminar BL, the AMI equation also has an intuitive physical explication in terms of torques that reshape the mean velocity profile, changing its angular momentum (moment of momentum) and affecting the slope at the wall (i.e., the skin friction).

This paper builds on the moment-of-momentum (or angular momentum) integral theory of Ref. [19], with extension to the heat transfer (passive scalar transport) for low-Mach-number BL flows. For high-speed BLs, the first-moment type integral equations for skin friction and surface heat flux are derived and examined on fully turbulent datasets [20]. A simultaneous accounting of how flow phenomena within the BL combine to set the skin friction and surface heat transfer provides a route for deeper understanding and potential engineering gains for controlling friction losses and heat transfer. The integral equations are herein concretely demonstrated as valuable analysis tools for interpreting the role of various flow phenomena influencing the skin friction and surface heat transfer, particularly during the transition to turbulence where the mean skin friction and surface heat flux reach to maximum. This paper is organized as follows. Section II summarizes the AMI equation, and the approach is logically extended to surface heat flux by introducing the moment of enthalpy integral (MEI) equation in Sec. III. In Sec. IV we apply the AMI and MEI equations to direct numerical simulation dataset of an incompressible BL with heat transfer undergoing bypass transition to turbulence [21]. Finally, conclusions and potential ideas for future work are reported in Sec. V.

II. Angular Momentum Integral Equation

The AMI equation quantifies how the flow phenomena influence BL skin friction in terms of "torques" redistributing (the deficit of) momentum in the wall-normal direction. In this context, the labeling of torque and angular momentum is done within the BL approximation in which the streamwise direction is time-like. Thus, only the wall-normal offset of forces and momentum is considered. Thus, the rate of change (d/dx) of net angular momentum is equal to the torque of the wall shear stress summed together with other torques due to inertial, viscous, pressure, and turbulent stresses. The AMI equation provides a global accounting of the skin friction in terms of flow torques that reshape the mean velocity profile as sketched in Fig. 1; these other torques reshape the mean velocity profile in the BL by transporting momentum (deficit) in the wall-normal direction, increasing or decreasing the skin friction coefficient depending on the sign of the torque. As depicted, a counterclockwise torque speeds up the near-wall flow at the expense of the outer region of the BL, leading to a higher skin friction coefficient. A good example of this effect is the Reynolds shear stress in a turbulent BL. Alternatively, a clockwise torque slows down the flow in the near-wall region and speeds up the outer region, decreasing the skin friction. An example of this is the torque of an adverse pressure gradient. These examples will be made clear in a mathematical sense as the AMI equation is developed in this section.

The derivation of the AMI equation proceeds similarly to von Kármán's momentum integral equation [22]. For the present work, the statistically two-dimensional mean flow in a flat-plate BL is described in Cartesian coordinates by the streamwise, $\overline{u}(x, y, t)$, and wall-normal, $\overline{v}(x, y, t)$, velocities, respectively. The Reynolds-averaged Navier–Stokes (RANS) equations for incompressible BLs —in a conservative form—read

$$\frac{\partial \overline{u}}{\partial x} + \frac{\partial \overline{v}}{\partial y} = 0 \tag{1}$$

for the mass and

$$\frac{\partial \overline{u}}{\partial t} + \frac{\partial (\overline{u}^2)}{\partial x} + \frac{\partial (\overline{u}\,\overline{v})}{\partial y} = -\frac{1}{\rho}\frac{\partial \overline{p}}{\partial x} + \nu\frac{\partial^2 \overline{u}}{\partial x^2} + \nu\frac{\partial^2 \overline{u}}{\partial y^2} - \frac{\partial \overline{u'u'}}{\partial x} - \frac{\partial \overline{u'v'}}{\partial y} \tag{2}$$

for the streamwise momentum conservations, respectively. In Eq. (2) the fluid's density ρ and kinematic viscosity ν remain constant. Also, $\overline{p}$ is the mean pressure. The effect of surface curvature on BLs can be neglected in some cases. Generalization of this approach to include BLs on surface with significant curvature effects is a topic for future work.

The BL is subjected from above to a freestream flow with velocity $U_\infty(x, t)$ and pressure $P_\infty(x, t)$, where x is the streamwise coordinate

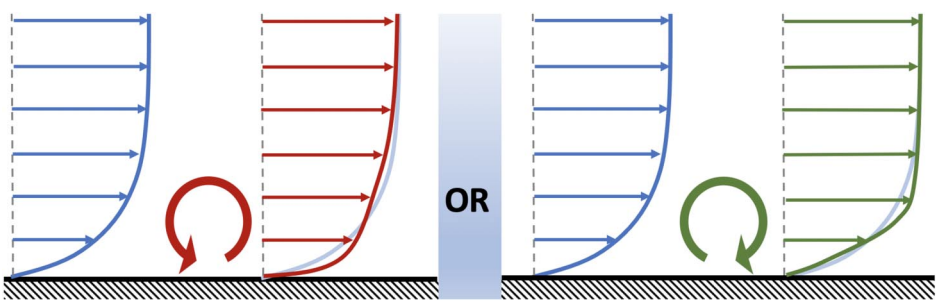

Fig. 1 On the left, a counterclockwise torque (e.g., Reynolds shear stress) transports momentum toward the wall, increasing the skin friction. On the right, the opposite occurs (e.g., an adverse pressure gradient).

along the surface. Within the freestream, the streamwise momentum equation is

$$\frac{\partial U_\infty}{\partial t} + U_\infty \frac{\partial U_\infty}{\partial x} = -\frac{1}{\rho}\frac{\partial P_\infty}{\partial x} \tag{3}$$

It is assumed here that wall-normal variation of U_∞ on the scale of the BL thickness is insignificant compared to the wall-normal variation of the velocity within the BL, though this assumption may need to be relaxed in the future to apply this approach to strong adverse pressure gradients and BL separation.

Now, subtracting Eq. (2) from Eq. (3) yields a transport equation for the streamwise momentum deficit $(U_\infty - \overline{u})$ as

$$\frac{\partial((U_\infty - \overline{u})\overline{u})}{\partial x} + \frac{\partial((U_\infty - \overline{u})\overline{v})}{\partial y} + (U_\infty - \overline{u})\frac{\partial U_\infty}{\partial x} = -\nu\frac{\partial^2 \overline{u}}{\partial y^2} + \frac{\partial \overline{u'v'}}{\partial y} - I_M \tag{4}$$

where all the terms neglected in statistically stationary high-Reynolds-number BL theory to the skin-friction coefficient are gathered in a single term:

$$I_M = \frac{\partial}{\partial t}(U_\infty - \overline{u}) + \frac{\partial}{\partial x}\left(-(\overline{u'u'}) + \nu\frac{\partial \overline{u}}{\partial x}\right) - \frac{1}{\rho}\left(\frac{\mathrm{d}P_\infty}{\mathrm{d}x} - \frac{\mathrm{d}\overline{p}}{\mathrm{d}x}\right) \tag{5}$$

Equation (4) expresses how the streamwise momentum deficit in BLs changes because of the streamwise and wall-normal fluxes, freestream acceleration, pressure gradient, viscous transport, and Reynolds stresses. Integration of Eq. (4) across the BL from $y = 0$ to $y = \infty$ and normalizing by U_∞^2 yield the von Kármán momentum integral equation [22] that reads

$$\frac{C_f}{2} = \frac{\mathrm{d}\theta}{\mathrm{d}x} + \frac{2\theta + \delta^*}{U_\infty}\frac{\mathrm{d}U_\infty}{\mathrm{d}x} + \mathcal{I}_M \tag{6}$$

where the momentum and displacement thicknesses are defined, respectively, as

$$\theta \equiv \int_0^\infty \left(1 - \frac{\overline{u}}{U_\infty}\right)\frac{\overline{u}}{U_\infty}\,\mathrm{d}y, \qquad \delta^* \equiv \int_0^\infty \left(1 - \frac{\overline{u}}{U_\infty}\right)\mathrm{d}y \tag{7}$$

and $\mathcal{I}_M$ represents the contribution of all the negligible terms [inside I_M, Eq. (5)] to $C_f/2$. Also, the skin-friction coefficient for BLs is $C_f \equiv 2\overline{\tau_\mathrm{w}}/\rho U_\infty^2$, in which $\overline{\tau_\mathrm{w}} = \mu(\partial\overline{u}/\partial y)_{y=0}$ is the shear stress at the wall and $\mu = \rho\nu$ is the fluid's dynamic viscosity.

Note that Eq. (6) is valid for laminar, transitional, and fully turbulent flows. In other words, the influence of fluctuations, e.g., Reynolds shear stress, momentum flux, and hence skin friction, is implicit. Because turbulence only rearranges momentum in the wall-normal direction, it does not directly provide a source or sink for the integral of momentum (deficit). Instead, the impact of turbulence on Eq. (6) is to change the relationship between C_f and θ. To see the effect of turbulence explicitly, one must consider how momentum is distributed in the wall-normal direction, e.g., by considering moments of momentum.

The AMI equation is derived by multiplying Eq. (4) by $(y - \ell(x))$—as the first moment—and integrating in the wall-normal direction from $y = 0$ to $y = \infty$. This may then be stated in terms of the skin-friction coefficient with a subsequent division by ℓU_∞^2 that yields

$$\frac{C_f}{2} = \frac{1}{Re_\ell} + \frac{1}{\ell}\int_0^\infty \frac{-\overline{u'v'}}{U_\infty^2}\,\mathrm{d}y + \left(\frac{\mathrm{d}\theta_\ell}{\mathrm{d}x} - \frac{\theta - \theta_\ell}{\ell}\frac{\mathrm{d}\ell}{\mathrm{d}x}\right) + \frac{\theta_v}{\ell} + \left(\frac{2\theta_\ell + \delta_\ell^*}{U_\infty}\frac{\mathrm{d}U_\infty}{\mathrm{d}x}\right) + \mathcal{I}_{\ell,M} \tag{8}$$

where the left-hand side is the skin-friction coefficient and on the right-hand side there are several terms related to several physical flow phenomena. In Eq. (8), $Re_\ell = U_\infty\ell/\nu$ represents the Reynolds number based on the length scale $\ell(x)$, and $\mathcal{I}_{\ell,M}$ contains all terms neglected in BL theory [in Eq. (5)]. The angular momentum and displacement thicknesses are defined as

$$\theta_\ell \equiv \int_0^\infty \left(1 - \frac{y}{\ell}\right)\left(1 - \frac{\overline{u}}{U_\infty}\right)\frac{\overline{u}}{U_\infty}\,\mathrm{d}y, \qquad \delta_\ell^* \equiv \int_0^\infty \left(1 - \frac{y}{\ell}\right)\left(1 - \frac{\overline{u}}{U_\infty}\right)\mathrm{d}y \tag{9}$$

which collapse to $\theta_\ell = \theta$ and $\delta_\ell^* = \delta^*$ in the limit of $\ell \to \infty$. In fact, the AMI equation returns the von Kármán momentum integral equation when $\ell \to \infty$. The wall-normal momentum thickness is defined as

$$\theta_v \equiv \int_0^\infty \left(1 - \frac{\overline{u}}{U_\infty}\right)\frac{\overline{v}}{U_\infty}\,\mathrm{d}y \tag{10}$$

representing the integration of the mean wall-normal flux of the streamwise momentum deficit. Equation (8) represents the integral budget of mean angular momentum with respect to $y = \ell$, in the BL approximation where x is a time-like variable. It may also be called a first moment of momentum integral equation [23] (for historical context, see also [24]).

According to Ref. [19], the choice of $\ell(x)$ can be made to isolate the zero pressure gradient (ZPG) laminar skin friction coefficient in a single term of the AMI equation, $2/Re_\ell$. This choice allows the other terms in the equation to be straightforwardly interpreted as enhancement or attenuation of the skin friction compared to a laminar BL at a matching Reynolds number. The skin-friction coefficient of ZPG laminar BLs from Blasius solution [17] yields

$$\frac{C_f}{2} = \frac{1}{Re_\ell} = \frac{0.332}{\sqrt{Re_x}} = \frac{0.221}{Re_\theta} = \frac{0.571}{Re_{\delta^*}} = \frac{1.63}{Re_\delta} \tag{11}$$

which corresponds to

$$\ell(x) = 3.01\sqrt{\frac{\nu x}{U_\infty}} = 4.54\theta(x) = 1.75\delta^*(x) \tag{12}$$

Each of these relations represents a unique choice for the AMI equation. For example, the choice of $\ell \sim \sqrt{x}$ makes the first term equal to the skin friction of the Blasius BL at a given Re_x. In that case, the AMI equation expresses the BL skin friction relative to the laminar case at the same Re_x. Similarly, the choice $\ell \sim \theta$ makes the first term equal to the Blasius friction for a given Re_θ, and thus the AMI equation quantifies the skin friction relative to a laminar BL as the same Re_θ. Therefore, the ability to choose $\ell(x)$ provides flexibility for the analysis and clarity of interpretation. Due to the physical basis of the momentum thickness stemming from the von Kármán momentum integral equation (6), the results in this paper will use the AMI equation with the length scale $\ell \sim \theta$. Elnahhas and Johnson [19] briefly considered different choices for the length scale, and further insights from other choices are left for future work.

Once the choice of ℓ is made, the other terms may now be interpreted as changes to the skin friction relative to a Blasius BL having the same Re_ℓ. The second term in Eq. (8) accounts for how turbulent fluctuations (via the Reynolds stress) alter the skin friction coefficient. Unsurprisingly, a negative correlation between streamwise and spanwise fluctuations increases skin friction (Fig. 1). In the AMI equation, the contribution of the Reynolds shear stress to skin friction is unweighted as a function of wall-normal distance, so that the wake region of the BL contains most of this integral.

The third term on the right-hand side of Eq. (8) expresses the streamwise growth of the angular momentum thickness θ_ℓ relative to how quickly ℓ increases. The increase in ℓ is dictated by the choice of length scale to use for Eq. (12), e.g., $\ell \sim \sqrt{x}$ or $\ell \sim \theta$, where the

coefficient is set by the Blasius solution. Another way of thinking about the AMI equation is that an increase in angular momentum thickness must be equal to the sum of the skin friction torque along with the other torques represented on the right-hand side of Eq. (8).

The mean wall-normal velocity also redistributes streamwise momentum (deficit), reflected in the fourth term on the right-hand side of Eq. (8). In the case of a positive mean wall-normal velocity, momentum deficit is carried away from the wall. This may be thought of as a torque that decelerates the mean flow in the outer BL and speeds up the near-wall flow, increasing the skin friction.

Any freestream pressure gradient also acts as a torque on the BL velocity profile. As quantified by the fifth term on the right-hand side of Eq. (8), an accelerating freestream (favorable pressure gradient) acts to increase the skin friction coefficient while a decelerating freestream (adverse pressure gradient) does the opposite. Finally, the contribution of the terms neglected by BL approximation is accumulated in the sixth term. A comprehensive interpretation of each flow phenomenon in the AMI equation is provided in Ref. [19].

III. Moment of Enthalpy Integral Equation

The derivation and interpretation of the AMI equation for skin friction was given previously by Elnahhas and Johnson [19]. An analogy between skin friction and surface heat transfer has long been a staple of BL theory. In this section, we build on the approach of the AMI equation to introduce an analogous MEI equation for surface heat transfer.

A. Derivation

For incompressible flows, the averaged conservation equation for enthalpy provides an expression for how turbulence and other flow phenomena alter the Stanton number, and hence the Reynolds's analogy. For statistically stationary, two-dimensional BLs, without heating source/sink, and with constant fluid properties, the Reynolds-averaged conservation equation for thermal energy—written in terms of temperature, T—reads

$$\frac{\partial \overline{T}}{\partial t}+\frac{\partial(\overline{u}\,\overline{T})}{\partial x}+\frac{\partial(\overline{v}\,\overline{T})}{\partial y}=\alpha\frac{\partial^2\overline{T}}{\partial x^2}+\alpha\frac{\partial^2\overline{T}}{\partial y^2}-\frac{\partial(\overline{u'T'})}{\partial x}-\frac{\partial(\overline{v'T'})}{\partial y} \tag{13}$$

where α is the fluid's thermal diffusivity. Subtracting the adiabatic freestream (T_∞ is constant) enthalpy, equation

$$\frac{\partial T_\infty}{\partial t}+U_\infty\frac{\partial T_\infty}{\partial x}=0 \tag{14}$$

from Eq. (13) yields a transport equation for the mean excess enthalpy equation (often $T_\mathrm{w}\geq T_\infty$ in incompressible BLs) in terms of temperature as

$$\begin{aligned}&\frac{\partial((\overline{T}-T_\infty)\overline{u})}{\partial x}+\frac{\partial((\overline{T}-T_\infty)\overline{v})}{\partial y}-(U_\infty-\overline{u})\frac{\partial T_\infty}{\partial x}\\&\quad=\alpha\frac{\partial^2\overline{T}}{\partial y^2}-\frac{\partial(\overline{v'T'})}{\partial y}+I_T\end{aligned} \tag{15}$$

where all the terms neglected in statistically stationary, two-dimensional BL approximations are gathered in a single term:

$$I_T=\frac{\partial}{\partial t}(T_\infty-\overline{T})+\frac{\partial}{\partial x}\left(-(\overline{v'T'})+\alpha\frac{\partial\overline{T}}{\partial x}\right) \tag{16}$$

Integrating Eq. (15) in the wall-normal direction from $y=0$ to $y=\infty$, then normalizing by $U_\infty(T_\mathrm{w}-T_\infty)$ results in a Kármán-integral-type relation for the Stanton number [1]

$$St=\frac{\mathrm{d}\delta^h}{\mathrm{d}x}+\frac{\delta^h}{U_\infty}\frac{\mathrm{d}U_\infty}{\mathrm{d}x}+\frac{\delta^h}{T_\mathrm{w}-T_\infty}\frac{\mathrm{d}T_\mathrm{w}}{\mathrm{d}x}+\mathcal{I}_T \tag{17}$$

where δ^h is the enthalpy thickness,

$$\delta^h\equiv\int_0^\infty\frac{\overline{u}}{U_\infty}\left(\frac{\overline{T}-T_\infty}{T_\mathrm{w}-T_\infty}\right)\mathrm{d}y \tag{18}$$

representing the wall-normal integral of the streamwise flux of the enthalpy excess (or deficit) [25]. Moreover, $\mathcal{I}_T$ corresponds to the contributions of the negligible terms (I_T) to the Stanton number. The Stanton number for incompressible BLs is defined as

$$St\equiv\frac{q_\mathrm{w}}{\rho U_\infty c_p(T_\mathrm{w}-T_\infty)} \tag{19}$$

representing the nondimensional form of surface heat flux $\overline{q_\mathrm{w}}=-\kappa(\partial\overline{T}/\partial y)_{y=0}$, where $\kappa=\rho c_p\alpha$ and c_p are the fluid's thermal conductivity and constant specific heat capacity, respectively.

Note that the influence of turbulence in Eq. (17) is implicit because turbulence rearranges enthalpy (and momentum) in the wall-normal direction; it does not directly provide a source or sink. Instead, the impact of turbulence in Eq. (17) is to change the relationship between St and δ^h. To explicitly quantify the impact of turbulence on the surface heat transfer, one must consider how enthalpy is distributed in the wall-normal direction, e.g., by considering the first moment of the enthalpy equation.

Similar to the AMI equation, the MEI equation is obtained by multiplying Eq. (15) by $(y-\ell)$—the first moment—then integrating across the BL, $\int_0^\infty(y-\ell)[\cdot]\,\mathrm{d}y$. Normalizing the resulting by $\ell U_\infty(T_\mathrm{w}-T_\infty)$ yields the MEI equation

$$\begin{aligned}St=&\frac{1}{Pe_\ell}+\frac{1}{\ell}\int_0^\infty\frac{\overline{T'v'}}{U_\infty(T_\mathrm{w}-T_\infty)}\,\mathrm{d}y+\left(\frac{\mathrm{d}\delta^h_\ell}{\mathrm{d}x}-\frac{\delta^h-\delta^h_\ell}{\ell}\frac{\mathrm{d}\ell}{\mathrm{d}x}\right)+\frac{\delta^h_v}{\ell}\\&+\frac{\delta^h_\ell}{U_\infty}\frac{\mathrm{d}U_\infty}{\mathrm{d}x}+\frac{\delta^h_\ell}{T_\mathrm{w}-T_\infty}\frac{\mathrm{d}T_\mathrm{w}}{\mathrm{d}x}+\mathcal{I}_{\ell,T}\end{aligned} \tag{20}$$

where $Pe_\ell=1/(Pr\cdot Re_\ell)$ is the Péclet number, and $Pr=\nu/\alpha$; δ^h_ℓ and δ^h_v are the first moment of enthalpy thickness and wall-normal enthalpy thickness, respectively, defined as

$$\begin{aligned}\delta^h_\ell&\equiv\int_0^\infty\left(1-\frac{y}{\ell}\right)\frac{\overline{u}}{U_\infty}\left(\frac{\overline{T}-T_\infty}{T_\mathrm{w}-T_\infty}\right)\mathrm{d}y,\\\delta^h_v&\equiv\int_0^\infty\frac{\overline{v}}{U_\infty}\left(\frac{\overline{T}-T_\infty}{T_\mathrm{w}-T_\infty}\right)\mathrm{d}y\end{aligned} \tag{21}$$

Note that, in the limit of $\ell\to\infty$, the first moment of enthalpy thickness collapses to δ^h, and hence the MEI equation becomes the classic integral Eq. (17). In Eq. (20), $\mathcal{I}_{\ell,T}$ represents the contribution of the neglected terms (I_T) to the Stanton number based on the first moment integral approach. Note that a meaningful interpretation of the MEI equation depends on the choice of the length scale ℓ; an appropriate definition of ℓ is precisely discussed in Sec. III.B.

B. Interpretation

The right-hand side of the MEI equation (20) consists of different terms mapping different physical flow phenomena and quantifying how they alter the Stanton number. A summary of the physical interpretation of these terms is provided below and supplemented by a brief discussion of each flow phenomenon in the following paragraphs.

(I) $\frac{1}{Pe_\ell}\to$ surface heat flux of an equivalent *laminar* BL at matched Pe_ℓ,

(II) $\frac{1}{\ell}\int_0^\infty\frac{\overline{T'v'}}{U_\infty(T_\mathrm{w}-T_\infty)}\,\mathrm{d}y\to$ *turbulent flux* integral, turbulent transport of enthalpy,

(III) $\frac{\mathrm{d}\delta^h_\ell}{\mathrm{d}x}-\frac{\delta^h-\delta^h_\ell}{\ell}\frac{\mathrm{d}\ell}{\mathrm{d}x}\to$ *streamwise growth* of the first moment of enthalpy thickness,

(IV) $\frac{\delta^h_v}{\ell}\to$ flux by *mean wall-normal* transport,

(V) $\frac{\delta^h_\ell}{U_\infty}\frac{\mathrm{d}U_\infty}{\mathrm{d}x}\to$ *freestream pressure* gradient flux,

(VI) $\frac{\delta^h_\ell}{T_w - T_\infty}\frac{dT_w}{dx} \rightarrow$ flux by *wall temperature variation*, and
(VII) $\mathcal{I}_{\ell,T} \rightarrow$ heat flux due to *negligible terms*.

1. Diffusion Flux and the Laminar Stanton Number (I)

In the MEI equation, the Stanton number and the *laminar* surface heat flux are obtained from the wall-normal integration of the first moment of the diffusion flux in Eq. (15)

$$\int_0^\infty (y-\ell)\left[\alpha\frac{\partial^2\overline{T}}{\partial y^2}\right]dy = -\ell(T_w - T_\infty)U_\infty\left(St - \frac{1}{Pr\cdot Re_\ell}\right) \tag{22}$$

From Eq. (22), if ℓ is chosen such that $St = 1/Pr\cdot Re_\ell$ for a ZPG incompressible laminar BL, then the integral of total diffusion flux about $y = \ell(x)$ vanishes. Therefore, the length scale $\ell(x)$ mathematically connects two BLs, the BL to be analyzed (in this paper, transition to turbulent) and the baseline (ZPG) incompressible laminar BL. In other words, the *laminar* Stanton number in the MEI equation is isolated in $1/Pr\cdot Re_\ell$ with such a choice for $\ell(x)$. Because of the physical basis of Eq. (17), we tie the definition of the length scale $\ell(x)$ to the enthalpy thickness, $\ell(x) \sim \delta^h(x)$; hence for an (a ZPG) incompressible laminar BL

$$St = \frac{1}{Pr\cdot Re_\ell} = \frac{\alpha}{U_\infty(c_T\delta^h(x))} \tag{23}$$

where c_T is a constant determined by solving the self-similar laminar incompressible BL equations, e.g., Blasius solution. For incompressible flows, there is a Prandtl number dependency between proposed length scales in the AMI and MEI equations (approximated ratio of the thermal and momentum BL thickness $\delta_T/\delta \approx Pr^{-0.4}$, where δ_T and δ are the thermal and momentum BL thicknesses, respectively [25]). In particular, when $Pr = 1$, the length scale of the MEI equation is equal to the AMI equation's length scale (obtained from Blasius solution) $\ell(x) = 4.54\delta^h = 4.54\theta$ ($\delta_h = \theta$ in laminar regime), i.e., $c_T = 4.54$. Thus, the Reynolds number used for similarity with the baseline laminar BL is $Re_{\delta^h} = U_\infty\delta^h/\nu = Re_\theta$. Note that this equality is not perfectly valid for the transitional and turbulent flows. In other words, the turbulent transport mechanism is not exactly the same for enthalpy (scalar quantity) and momentum (vector quantity) fluxes.

2. Turbulent Enthalpy Flux (II)

The second term on the right-hand side of the MEI equation is the *turbulent flux* by wall-normal velocity temperature covariance, $\overline{v'T'}$. The turbulent heat flux does not appear directly in the Kármán-integral-type equation (17), since it vanishes at boundaries (wall and freestream). However, by integrating the first moment of the velocity–temperature covariance in the enthalpy excess equation

$$-\int_0^\infty (y-\ell)\frac{\partial(\overline{v'T'})}{\partial y}\,dy = \int_0^\infty \overline{v'T'}\,dy \tag{24}$$

the *turbulent flux* is preserved. The *turbulent flux* represents how turbulence carries enthalpy excess away from the wall, generating further heat flux relative to the base *laminar* heat flux.

3. Streamwise Growth of Moment-of-Enthalpy Thickness (III)

Integrating the first moment of the streamwise enthalpy excess yields

$$-\int_0^\infty (y-\ell)\frac{\partial}{\partial x}\left(\frac{\overline{u}}{U_\infty}\left(\frac{\overline{T}-T_\infty}{T_w - T_\infty}\right)\right)dy = \ell\frac{d\delta^h_\ell}{dx} - \left(\delta^h - \delta^h_\ell\right)\frac{d\ell}{dx} \tag{25}$$

The enthalpy thickness δ^h from the Kármán integral type equation (17) represents the net streamwise flux of enthalpy deficit/excess. Equation (25) represents the rate at which the first moment of enthalpy thickness grows relative to the growth rate of $\ell(x)$. The first moment of enthalpy thickness, δ^h_ℓ, is a signed quantity, and so it can be negative or positive depending on the choice of $\ell(x)$. A physical interpretation of Eq. (25) is considering it as the resultant term from all of the fluxes impacting the BL as well as the surface heat flux itself in the left-hand side of the MEI equation. In other words, the first moment of enthalpy thickness absorbs any imbalance of enthalpy fluxes at a given streamwise location. For example, it will be shown that this term is often negative (attenuation of surface heat flux). In this case, this streamwise growth term may be interpreted as absorbing the turbulent heat flux, which would otherwise necessitate a larger surface heat flux, into a growth of the moment of enthalpy.

4. Mean Wall-Normal Flux (IV)

The *mean wall-normal* flux in the MEI equation originates from the flux of enthalpy excess carried by the mean wall-normal velocity:

$$-\int_0^\infty (y-\ell)\frac{\partial}{\partial y}\left(\frac{\bar{v}}{U_\infty}\left(\frac{\overline{T}-T_\infty}{T_w - T_\infty}\right)\right)dy = \delta^h_v \tag{26}$$

This term represents the wall-normal flux of enthalpy. When $\overline{v}$ is positive, as is typically in BLs, this term increases the Stanton number by assisting the wall-normal transport of enthalpy away from the wall. Conversely, if $\overline{v} < 0$, the mean wall-normal velocity transports enthalpy excess toward the wall, attenuating the Stanton number. This reversal behavior is observed for transitional BLs in the AMI equation for the skin friction coefficient [19].

5. Flux by freestream Pressure Gradient (IV)

A nonzero freestream pressure gradient due to variable U_∞ with the streamwise direction impacts the surface heat flux. For instance, a favorable freestream pressure gradient accelerates U_∞, damping the velocity defect in the BL and contributing to the Stanton number, whereas an adverse freestream pressure gradient decreases the surface heat flux. In this paper, only zero freestream pressure gradient incompressible BL will be considered, and so this term is expected to be negligible. MEI-based analysis of pressure gradient effects on surface heat transfer is reserved for future work.

6. Flux by Non-Isothermal Wall (VI)

According to the MEI equation, wall temperature variation impacts the surface heat flux. Increasing wall temperature in the streamwise direction enhances the surface heat flux, yet diminishing wall temperature causes a negative contribution to the Stanton number. In this paper, the focus will be on isothermal BL; hence this term is going to be negligible. Analysis of BLs with wall temperature variation is left to future work.

7. Departure from the BL Approximations (VII)

All terms in the enthalpy excess transport equation that are typically small in statistically stationary and two-dimensional BLs are accumulated in a single term, the $\mathcal{I}_{\ell,T}$. While not the case in this paper, these terms could become considerable in the vicinity of flow separation.

IV. Numerical Results

The AMI equation and its extension to heat transfer, the MEI equation, are generally applicable analysis tools for BL flows; note that for incompressible flows with constant flow properties, like in this paper, enthalpy and temperature can be used interchangeably. They are demonstrated in this section for a transitional and turbulent flat plate BL with zero pressure gradient using data from a direct numerical simulation (DNS) by Wu et al. [21]. The simulation inlet is a laminar (Blasius) BL at $Re_\theta \approx 80$, with turbulence from a precursor simulation of homogeneous isotropic turbulence added to the freestream to trigger bypass transition. The inlet turbulent intensity in the freestream is 3%. The simulation domain is long enough in the streamwise direction, allowing the turbulent BL to grow to $Re_\theta \approx 3000$ and $Re_\tau \approx 1000$ at the outlet. A total of $16384 \times 500 \times 512$ grid

points are used. The temperature field (passive scalar) is simulated with $Pr = 1$ with isothermal boundary conditions at the wall. Standard DNS grid resolutions are used. More details about the simulation and grid resolution are given in Ref. [21].

A. AMI Equation for the Skin Friction

Preliminary results for the skin friction and the right-hand side of Eq. (8) are shown in Fig. 2. The right-hand side of the AMI equation balances the skin-friction coefficient with approximately 1.4% average error. The major cause of the deviation is the amplification of statistical convergence errors generated by calculating the derivatives in the streamwise direction in the *streamwise growth*. Also plotted are the skin friction formulae from the Blasius solution, $0.442/Re_\theta$, and a power-law approximation for turbulent BLs, $0.026/Re_\theta^{0.25}$. According to these results, the skin friction deviates from the laminar solution at approximately $Re_\theta = 200$, and the flow becomes fully turbulent at roughly $Re_\theta = 900$.

In Figs. 3a and 3b, the contributions of the four major terms on the right-hand side of the AMI equation to the skin-friction coefficient are shown with respect to Re_θ. The AMI equation's length scale $\ell(x) = 4.54\theta(x)$ based on the Blasius solution. Note that the DNS simulation has a nominal zero freestream pressure gradient and is far from BL separation. Therefore, the contribution of these two AMI terms to the skin-friction coefficient is orders of magnitude smaller than the other four terms. Figure 3a exhibits the direct impact of the first four terms on $C_f/2$, and Fig. 3b provides their normalized contribution by $C_f/2$.

For $Re_\theta < 200$, where the flow is mostly laminar, the dominant flow phenomenon in the AMI equation generating friction is the *laminar* term. The *laminar* friction, however, decreases downstream with $\sim 1/\sqrt{x}$ in the streamwise direction. During the initial stages of transition, the fluctuations (or perturbations) are significantly weak; hence, the enhancement of *turbulent torque* to $C_f/2$ is negligible. In contrast, for the fully turbulent regime ($Re_\theta > 900$), the contribution of *turbulent torque* to $C_f/2$ is dominant because most of the wall-normal momentum transport is done by Reynolds shear stress that brings high-speed flow toward the wall. According to Fig. 3b, the normalized contribution of *turbulent torque* is about one, confirming roughly that all of the wall-normal transport mechanism is done by Reynolds shear stress.

The *streamwise growth* in angular momentum thickness is an overall negative contribution to the skin friction because this represents that the mean velocity profile of the BL absorbs angular momentum as it becomes thicker, offsetting the torques and decreasing the required skin friction needed to balance the integral equation. The mean wall-normal velocity is usually positive as the BL grows so that θ_v is positive in the laminar and fully turbulent regimes. Thus, the mean transport of momentum deficit away from the wall provides torque in the direction requiring a larger skin friction coefficient. However, the contribution of *mean-wall normal* is generally weaker than the aforementioned dominant terms in the laminar and turbulent regimes.

Within the laminar regime ($Re_\theta < 200$) the *mean-wall normal* and *streamwise growth* balance each other so that their sum is zero by design. That is, the choice of ℓ ensures that streamwise growth precisely offsets the wall-normal velocity of the Blasius BL. For fully turbulent BL ($Re_\theta > 900$), also, the normalized contribution of these two flow phenomena to $C_f/2$ in Fig. 3b is small and relatively constant. In fact, beyond $Re_\theta \approx 1200$, none of the terms in the AMI equation vary significantly in relative magnitude. Therefore, from the perspective of the AMI equation, the basic physics of skin friction enhancement by turbulence can be understood at relatively modest Reynolds numbers. For the remainder of this paper, the focus will be on the behavior of the four major flow phenomena in the AMI and MEI equations during the transition to turbulence and early turbulent regime ($Re_\theta \leq 1200$).

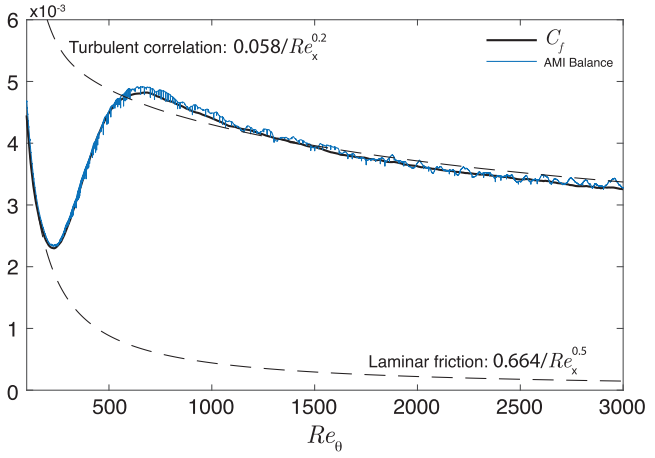

Fig. 2 The balance of the right-hand side of the AMI equation compared with C_f. The labeled dashed curves are laminar (Blasius) friction and turbulent correlation of skin-friction coefficient [25].

B. MEI Equation for Surface Heat Flux

In this section, the MEI equation is applied to analyze the mean surface heat flux in the BL database from Ref. [21]. The balance of the right-hand side of the MEI equation is compared with the left-hand side (the Stanton number) in Fig. 4 within the transitional and early turbulent regime ($Re_\theta \leq 1200$). The average error is approximately 1.3%, approximately the same as observed for the AMI equation in Fig. 2.

The DNS simulation has an adiabatic freestream condition with zero pressure gradient, and isothermal wall boundary condition is imposed. Hence, the contributions of *edge pressure gradient flux*, and *wall temperature variation* to the Stanton number are found to be negligible, as expected. In addition, the BL is away from any flow separations, so the BL approximations are valid, resulting in a substantially small effect from the *negligible terms* on surface heat flux. In Figs. 5a and 5b the four major flow phenomena in the right-hand side of the MEI equation with respect to $Re_\delta^h = U_\infty \delta^h/\nu$ are shown. The MEI equation's length scale, $\ell(x) = 4.54\delta^h(x)$, is the same as the AMI equation for $Pr = 1$. Figure 5a shows the direct contribution of each term to St, and Fig. 5b provides their relative contribution (each term normalized by St). Given the DNS data for $Pr = 1$ (and

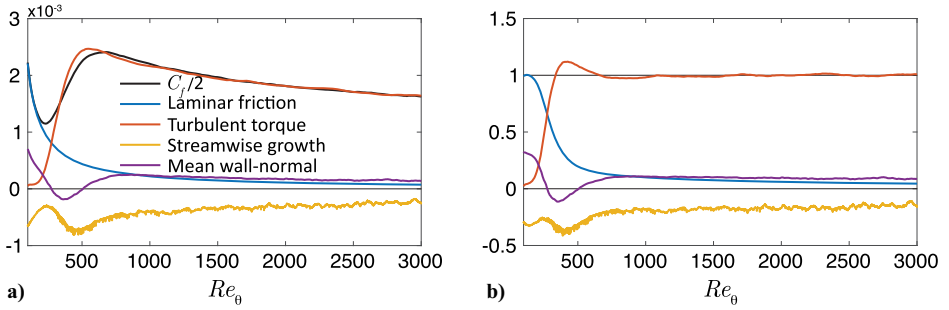

Fig. 3 The AMI budget for the four significant flow phenomena with respect to Re_θ: a) the contribution of each term to $C_f/2$, and b) the contribution of each term normalized by $C_f/2$.

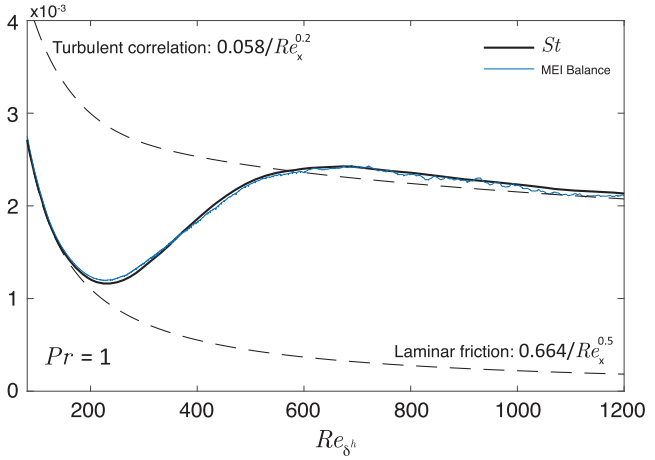

Fig. 4 The balance of the right-hand side of the MEI equation compared with St. The labeled dashed curves are laminar Stanton number and turbulent power-law prediction of the Stanton number [25].

$Re_\theta \approx Re_\delta^h$) the Reynolds analogy is expected and, qualitatively observed by comparing Figs. 5a and 5b and Figs. 3a and 3b for the MEI and AMI equations, respectively. Quantitatively, however, we spot a deviation in Reynolds analogy, especially within the fully turbulent regime; downstream of $Re_\theta = 900$, the explicit turbulence enhancement to the Stanton number is greater than its counterpart contribution to the skin friction coefficient. This deviation is more clear comparing the value of the normalized contribution of *turbulent flux* to St and *turbulent flux* to $C_f/2$ (Figs. 3b and 5b); for the *turbulent torque* it yields one, whereas for the *turbulent flux* it is about 10% higher. The main explanation for this deviation is the slight difference between the turbulent transport mechanism for a scalar quantity (enthalpy/temperature) and a divergence-free vector quantity (momentum/velocity).

Within the laminar region (early transition), $Re_\theta < 200$, the fractional contribution of the *laminar* heat flux is about one—verifying that this term properly represents the laminar heat flux—while the *streamwise growth* and *mean wall-normal* flux precisely offset each other by design. For fully turbulent flow, the *laminar* Stanton number is insignificant, and the surface heat flux generated directly by turbulence is slightly higher than the net Stanton number. Therefore, there must be (at least) one term resisting the turbulent heat flux. Similar to the AMI analysis, the *streamwise growth* negatively contributes to St. That is, it absorbs the impact of turbulence into a growth in the moment of enthalpy. According to Fig. 5b since the normalized enhancement of *turbulent flux* is somehow converged, the normalized negative contribution of *streamwise growth* does not vary significantly downstream. Moreover, the relatively small positive mean wall-normal velocity assists the wall-normal transport of enthalpy; hence *mean wall-normal* flux weakly contributes to the enhancement of the mean Stanton number.

Whereas for the laminar and fully turbulent BLs (away from separation) the balance of the MEI and AMI equations follow the fundamental physical expectations, during the transition and early turbulent we observe an unexpected trend by the major flow phenomena resulting in the maximum surface heat flux and skin friction. The transitional BL is explored in more detail in Sec. IV.C by considering the MEI and AMI equations together.

C. Peak Surface Friction and Heat Flux During the Transition to Turbulence

In this section, the peak surface heat flux and friction during the transition are examined by applying the physical understanding of the MEI and AMI equations. As the transition initiates ($Re_\theta > 200$), the *turbulent flux* boosts up and outpaces St beyond $Re_\theta \approx 380$ (Fig. 5). A similar trend is observed for the *turbulent torque* in the AMI equation, but the outpacing is temporal, confined between $Re_\theta \approx 380$ and $Re_\theta \approx 1000$ (Fig. 3). The integral of $-\overline{u'v'}$ reaches its peak value roughly at $Re_\theta \approx 530$. With a slight spatial delay, the maximum St and $C_f/2$ occur roughly at $Re_\theta \approx 650$. Surprisingly, in contrast to the laminar regime, during the transition, the *streamwise growth* and *mean wall-normal* cooperate, resisting the severe turbulent enhancement of surface heat flux and friction. To examine the (stronger) negative contribution of these two flow phenomena, we examine the contours of the integrands of *turbulent flux* (and *turbulent torque*), *mean wall-normal*, and *streamwise growth* in the x–y plane in the following paragraphs.

The direct impact of turbulence on St (and $C_f/2$) relative to the laminar effect is through the wall-normal integral of the turbulent covariance. Figures 6a and 6b exhibit the contour plots of the

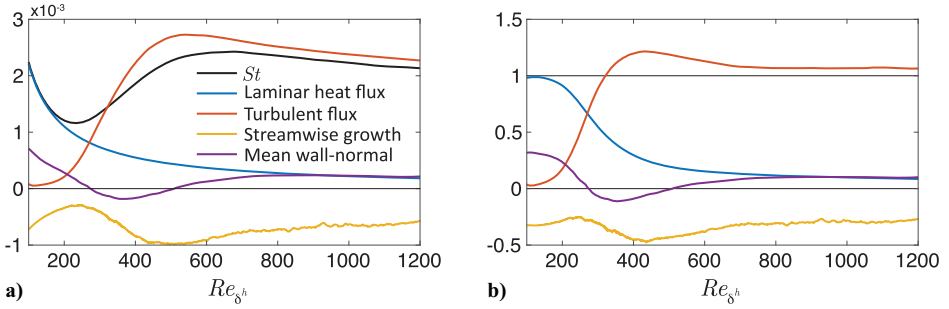

Fig. 5 The MEI budget for the four significant flow phenomena with respect to Re_θ: a) the contribution of each term to St, and b) the contribution of each term normalized by St.

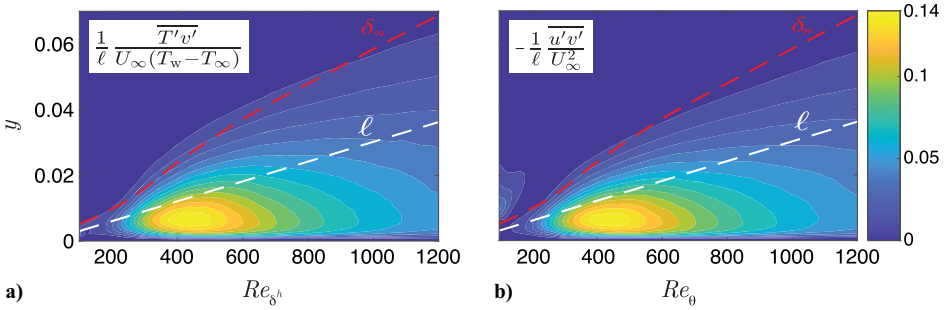

Fig. 6 Integrands of the explicit turbulence enhancement on the a) Stanton number by $\overline{T'v'}/\ell U_\infty(T_w - T_\infty)$, and b) skin-friction coefficient by $-\overline{u'v'}/\ell U_\infty^2$.

turbulent heat flux, $\overline{v'T'}$, and Reynolds shear stress, $-\overline{u'v'}$, normalized by $U_\infty(T_w - T_\infty)$ and U_∞^2, respectively. These two are the integrands of the associated terms in the AMI and MEI equations. The Reynolds stress and heat flux reach a maximum during transition in a region close to the wall, $y < \ell$, approximately from $Re_\theta = 380$ to $Re_\theta = 550$, where the turbulent covariance is substantially high and reaches the maximum within a localized region (yellow). This region coincides with the maximum contribution of *turbulent heat flux* (and *turbulent torque*) to *St* and $C_f/2$, and is slightly higher for the former than the latter, explaining the higher contribution of *turbulent flux* to *St* compared with the contribution of *turbulent torque* to $C_f/2$ in Figs. 3 and 5.

For laminar or fully turbulent regimes, the *mean wall-normal* velocity is positive and thus increases *St* (and $C_f/2$) by assisting in the transport of temperature excess (or velocity deficit) away from the wall. During transition to turbulence ($230 \le Re_\theta \le 680$), however, the wall-normal velocity $\overline{v}$ switches sign to negative in a region near the wall, as shown in Fig. 7b. When $\overline{v} < 0$, the contribution of the *mean wall-normal* flux to *St* (and $C_f/2$) is negative. This effect can be observed in Fig. 7c within the range of $300 \le Re_\theta \le 500$.

The authors are not aware of previous research exploring the observed negative wall-normal velocity during transition, so a short explanation is pursued here. The conservation of mass in an incompressible flow constrains the mean velocity field to be divergence free [Eq. (1)]. As a laminar or fully turbulent BL grows, the near-wall flow typically decelerates in a gradual manner, $\partial\overline{u}/\partial x < 0$. During transition to turbulence, however, the introduction of coherent transitional structures rapidly mixes higher speed fluid toward the wall. This accelerates the near-wall flow in the streamwise direction, i.e., $\partial\overline{u}/\partial x \ge 0$, as shown in Fig. 8a. To satisfy the continuity constraint, $\partial\overline{v}/\partial y \le 0$ in this near-wall region (Fig. 8b). Given the no-penetration boundary condition that $v = 0$ at the wall, the wall-normal velocity must therefore be toward the wall to accommodate the localized streamwise acceleration. Thus, the mean wall-normal transport of momentum and heat (temporarily) reverses direction. The impact of this reversal on skin-friction and surface heat transfer is quantified in Fig. 7c. In Figs. 5 (and Fig. 3), the contribution of the *turbulent flux* (and *turbulent torque*) demonstrates an inflection point (a curvature change)—at about $Re_\theta = 380$—during the transition. This curvature change corresponding to the streamwise location where the turbulent enhancement growth weakens that coincides with the negative contribution of *mean wall-normal* during the transition as well as the stronger streamwise growth of the BL thickness.

The other flow phenomena influencing the turbulence enhancement of surface heat transfer (and skin-friction) is the streamwise growth of the first moment of enthalpy thickness (or angular momentum thickness). This flow phenomenon has a negative contribution in incompressible BLs away from flow separation to skin friction [19] and surface heat flux (see Figs. 3 and 5). For laminar flows, the streamwise growth term in AMI and MEI is negative with

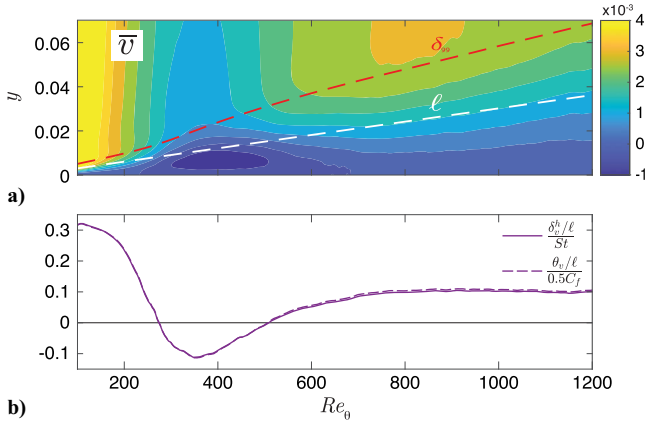

Fig. 7 Impact of the *mean wall-normal* flux to the AMI and MEI analysis. a) Contour plot of wall-normal velocity in the *x*–*y* plane, and b) the direct contribution of the *mean wall-normal* flux to *St* and $C_f/2$.

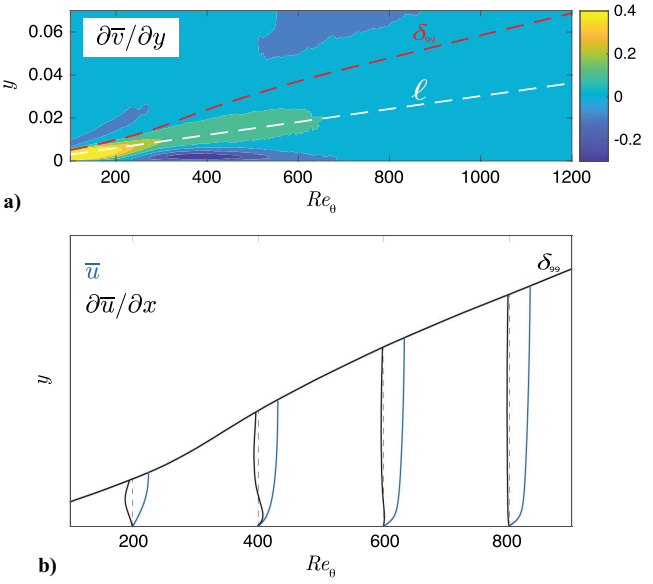

Fig. 8 a) Contour plot of the mean wall-normal velocity acceleration in *y*, and b) profiles of the streamwise velocity and (spatial) streamwise acceleration ($\partial\overline{u}/\partial x$) within transitional BL.

decaying magnitude. During transition, the negative contribution of the *streamwise growth* to *St* (and $C_f/2$) grows in magnitude from $Re_\theta = 230$ to $Re_\theta = 500$ (at the peak *turbulent flux*), partially offsetting the sharp increase in the turbulent heat flux. Downstream of $Re_\theta = 500$, when the near-wall streamwise velocity gradually decelerates in the streamwise direction, the effect of *streamwise growth* slowly drops. In Figs. 9a and 9b, contours of the integrands of the *streamwise growth* for the MEI and AMI equations are shown, corresponding to a quantitative mapping based on its effect on the surface flux quantities. During the transition (from $Re_\theta \approx 230$ to $Re_\theta \approx 680$), a reversed behavior in the integrand of the *streamwise growth* is observable near the wall, corresponding to the region where the near-wall flow accelerates in the streamwise direction (Fig. 8). Note that $\partial\overline{u}/\partial x$ is a crucial term in the integrands. Therefore, the higher the streamwise acceleration, the greater the negative contribution of *streamwise growth* to *St* (and $C_f/2$).

To summarize, in the transitional region there are several flow aspects involved in a rapid process to increase the Stanton number (and skin-friction coefficient). The dominant effect is simply the significant increase in momentum and enthalpy transport by rapidly growing instabilities. Other phenomena of the flow above the wall tend to partially offset the impact of the enhanced transport on surface flux quantities. Specifically, the *mean wall-normal* flux and *streamwise growth* of BL thickness act in a manner to attenuate skin friction and surface heat flux, mitigating the turbulence's impact. For the fully turbulent flow, the dominant flow phenomenon generating skin friction and heat transfer at the wall is the turbulent heat flux, while the other terms involved in Eq. (20) have a relatively small effect, without significant streamwise variation, merely balancing each other.

V. Conclusions

The turbulent enhancement of the surface friction and heat transfer is implicit in the classic Kármán-type integral equations for BL flows. This paper introduced a new MEI equation to quantify the impact of various flow phenomena on the Stanton number of incompressible BL flows. Analogous to the AMI equation of Elnahhas and Johnson [19], the MEI equation is developed using the first moment of the excess enthalpy (or temperature) equation and explicitly quantifies the impact of turbulent transport on surface heat transfer as an integral of the turbulent heat flux. More generally, the MEI equation provides a quantifying mapping of BL flow phenomenon based on how they alter the surface heat flux. The MEI equation represents a comparison of a turbulent BL with an equivalent laminar one, which is represented by the first term on the right-hand side. As such, other

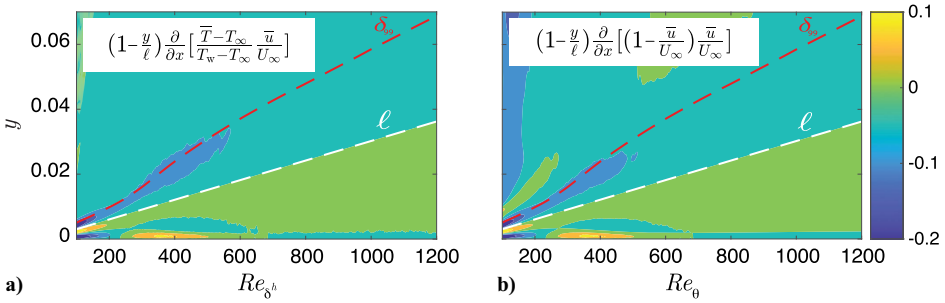

Fig. 9 Contour plots of the integrands of the *streamwise growth*: a) in the MEI equation for St; b) in the AMI equation for $C_f/2$.

terms affecting the surface heat flux are cleanly interpreted as changes relative to the surface heat flux of the equivalent laminar BL case.

The use of the AMI and MEI equations as incisive analysis tools was demonstrated on a DNS database of a transitional and turbulent BL. Through the transition to turbulence, the rapid growth of the turbulent heat flux is quantitatively mapped to its influence on surface heat flux, while the MEI equation reveals how mean wall-normal and streamwise growth terms are both resisting the turbulence enhancement of the Stanton number. A closer look at the mean flow reveals how the Reynolds shear stress accelerates the near-wall flow. This phenomenon results in two effects. First, the streamwise positive acceleration near the wall causes the moment of enthalpy thickness to grow faster, absorbing more of the turbulent heat flux into a reshaping of the mean enthalpy (or temperature) profile. Second, the near-wall flow acceleration induces a negative mean wall-normal velocity to satisfy continuity. This negative wall-normal flux due to the mean velocity temporarily opposes the action of the turbulent heat flux in re-arranging the distribution of the thermal energy in the BL. In a fully turbulent flow, the dominant enhancement of Stanton number (and skin-friction coefficient) is quantified as the integral of the turbulent heat (and momentum) flux, while the contribution of other flow phenomena in the MEI (and AMI) equation is relatively smaller, and asymptote (to our knowledge). In conclusion, the MEI and AMI equations provide a flexible, intuitive framework for quantitatively connecting flow phenomena throughout the BL to their effect on the surface heat flux and skin friction, respectively. While this analysis tool is demonstrated only for a relatively simple flow in this paper, it opens up the possibility of using this approach for many other applications and purposes in future work. For example, the AMI and MEI equations are suitable for analysis of BLs subjected to freestream pressure gradients, and they may be adapted to account for surface curvature effects. The design and optimization of flow control schemes aiming to decrease skin friction, delay transition, or alter surface heat transfer may benefit from the quantitative nature of the insight provided by the AMI and MEI equations. For future studies, this concept can be extended to incorporate how different turbulent length scales are responsible for the turbulent enhancement, connecting turbulence structure with engineering quantities of interest.

Acknowledgments

The authors thank X. Wu for sharing the direct numerical simulation dataset analyzed in this paper. P. L. Johnson thanks A. Lozano-Duran for initial discussions that motivated this work. Ahmed Elnahhas acknowledges support from NASA under Grant No. 80NSSC20M0201.

References

[1] Schlichting, H., and Kestin, J., *Boundary Layer Theory*, Vol. 121, Springer, Berlin, 1961, Chaps. 15 and 16.

[2] Kleiser, L., and Zang, T. A., "Numerical Simulation of Transition in Wall-Bounded Shear Flows," *Annual Review of Fluid Mechanics*, Vol. 23, No. 1, 1991, pp. 495–537. https://doi.org/10.1146/annurev.fl.23.010191.002431

[3] Wang, T., Keller, F., and Zhou, D., "Flow and Thermal Structures in a Transitional Boundary Layer," *Experimental Thermal and Fluid Science*, Vol. 12, No. 3, 1996, pp. 352–363. https://doi.org/10.1016/0894-1777(95)00126-3

[4] Durbin, P., and Wu, X., "Transition Beneath Vortical Disturbances," *Annual Review of Fluid Mechanics*, Vol. 39, No. 1, 2007, pp. 107–128. https://doi.org/10.1146/annurev.fluid.39.050905.110135

[5] Simpson, R. L., "Turbulent Boundary-Layer Separation," *Annual Review of Fluid Mechanics*, Vol. 21, No. 1, 1989, pp. 205–232. https://doi.org/10.1146/annurev.fl.21.010189.001225

[6] Choi, H., Moin, P., and Kim, J., "Active Turbulence Control for Drag Reduction in Wall-Bounded Flows," *Journal of Fluid Mechanics*, Vol. 262, Oct. 1994, pp. 75–110. https://doi.org/10.1017/S0022112094000431

[7] Bewley, T. R., Moin, P., and Temam, R., "DNS-Based Predictive Control of Turbulence: An Optimal Benchmark for Feedback Algorithms," *Journal of Fluid Mechanics*, Vol. 447, Nov. 2001, pp. 179–225. https://doi.org/10.1017/S0022112001005821

[8] Wang, M., and Zaki, T. A., "State Estimation in Turbulent Channel Flow from Limited Observations," *Journal of Fluid Mechanics*, Vol. 917, June 2021, p. A9. https://doi.org/10.1017/jfm.2021.268

[9] Fukagata, K., Iwamoto, K., and Kasagi, N., "Contribution of Reynolds Stress Distribution to the Skin Friction in Wall-Bounded Flows," *Physics of Fluids*, Vol. 14, No. 11, 2002, pp. L73–L76. https://doi.org/10.1063/1.1516779

[10] Bannier, A., Garnier, E., and Sagaut, P., "Riblet Flow Model Based on an Extended FIK Identity," *Flow, Turbulence and Combustion*, Vol. 95, No. 2, 2015, pp. 351–376. https://doi.org/10.1007/s10494-015-9624-2

[11] Peet, Y., and Sagaut, P., "Theoretical Prediction of Turbulent Skin Friction on Geometrically Complex Surfaces," *Physics of Fluids*, Vol. 21, No. 10, 2009, Paper 105105. https://doi.org/10.1063/1.3241993

[12] Nobuhide, K., Yosuke, H., Koji, F., and Kaoru, I., "Control of Turbulent Transport: Less Friction and More Heat Transfer," *Journal of Heat Transfere*, Vol. 134, No. 3, 2012. https://doi.org/10.1115/1.4005151

[13] Kim, J., "Physics and Control of Wall Turbulence for Drag Reduction," *Philosophical Transactions of the Royal Society A: Mathematical, Physical and Engineering Sciences*, Vol. 369, No. 1940, 2011, pp. 1396–1411. https://doi.org/10.1098/rsta.2010.0360

[14] Mehdi, F., and White, C. M., "Integral Form of the Skin Friction Coefficient Suitable for Experimental Data," *Experiments in Fluids*, Vol. 50, Jan. 2011, pp. 43–51. https://doi.org/10.1007/s00348-010-0893-1

[15] Mehdi, F., Johansson, T. G., White, C. M., and Naughton, J. W., "On Determining Wall Shear Stress in Spatially Developing Two-Dimensional Wall-Bounded Flows," *Experiments in Fluids*, Vol. 55, Jan. 2014, pp. 1–9. https://doi.org/10.1007/s00348-013-1656-6

[16] Xia, Q.-J., Huang, W.-X., Xu, C.-X., and Cui, G.-X., "Direct Numerical Simulation of Spatially Developing Turbulent Boundary Layers with Opposition Control," *Fluid Dynamics Research*, Vol. 47, No. 2, 2015, Paper 025503. https://doi.org/10.1088/0169-5983/47/2/025503

[17] Blasius, H., *Grenzschichten in Flüssigkeiten mit kleiner Reibung*, Druck von BG Teubner, 1907.

[18] Renard, N., and Deck, S., "A Theoretical Decomposition of Mean Skin Friction Generation into Physical Phenomena Across the Boundary

Layer," *Journal of Fluid Mechanics*, Vol. 790, March 2016, pp. 339–367. https://doi.org/10.1017/jfm.2016.12

[19] Elnahhas, A., and Johnson, P. L., "On the Enhancement of Boundary Layer Skin Friction by Turbulence: An Angular Momentum Approach," *Journal of Fluid Mechanics*, Vol. 940, June 2022, p. A36. https://doi.org/10.1017/jfm.2022.264

[20] Kianfar, A., Di Renzo, M., Williams, C., Elnahhas, A., and Johnson, P. L., "Angular Momentum and Moment of Total Enthalpy Integral Equations for High-Speed Boundary Layers," *Physical Review Fluids*, Vol. 8, No. 5, Paper 054603, May 2023, p. 34. https://doi.org/10.1103/PhysRevFluids.8.054603

[21] Wu, X., Moin, P., Wallace, J. M., Skarda, J., Lozano-Durán, A., and Hickey, J.-P., "Transitional–Turbulent Spots and Turbulent–Turbulent Spots in Boundary Layers," *Proceedings of the National Academy of Sciences*, Vol. 114, No. 27, 2017, pp. E5292–E5299. https://doi.org/10.1073/pnas.1704671114

[22] von Kármán, T., "Uber Laminare und Turbulente Reibung," *Zeitschrift für Angewandte Mathematik und Mechanik*, Vol. 1, No. 4, 1921, pp. 233–252.

[23] Johnson, P., "Toward Evaluating Contributions to Skin Friction Enhancement by Transition and Turbulence in Boundary Layer Flows," *Annual Research Briefs 2019*, Stanford University, Stanford, CA, 2019, pp. 223–235.

[24] Kline, S. J., Morkovin, M. V., Sovran, G., and Cockrell, D. J., "Computation of turbulent boundary layers," *AFOSR-IFP-Stanford Conference*, Stanford, CA, 1968.

[25] White, F., *Viscous Fluid Flow*, McGraw–Hill International Edition, McGraw–Hill, New York, 2006, Chap. 4.

P. Durbin
Associate Editor